Impurity charge compensation in graphene by a polarized ferroelectric polymer and its effect on charge transport near the Dirac point

Cite as: AIP Advances 11, 085015 (2021); doi: 10.1063/5.0054083
Submitted: 20 July 2021 • Accepted: 27 July 2021 •
Published Online: 9 August 2021

Kelotchi S. Figueroa,[1] Natalya A. Zimbovskaya,[1] Nicholas J. Pinto,[1,a)] Chengyu Wen,[2] and A. T. Charlie Johnson[3]

AFFILIATIONS

[1] Department of Physics and Electronics, University of Puerto Rico, Humacao, Puerto Rico 00791, USA
[2] Electrical and Systems Engineering, University of Pennsylvania, Philadelphia, Pennsylvania 19104, USA
[3] Department of Physics and Astronomy, University of Pennsylvania, Philadelphia, Pennsylvania 19104, USA

[a)] **Author to whom correspondence should be addressed:** nicholas.pinto@upr.edu

ABSTRACT

Charge transport near the Dirac point (DP) was investigated in graphene using ferroelectric (FE) gating in the temperature range of 300 < T < 350 K. We observed that the conductivity (σ) near the DP had a positive temperature gradient that switched to a negative temperature gradient with increasing temperature. The switch to a negative temperature gradient shifted to higher temperatures and gradually weakened upon moving away from the DP. Impurity charge compensation via polarization of the FE together with a temperature-dependent graphene–impurity charge separation was proposed as being responsible for the non-monotonicity in σ(T). A self-consistent theory for graphene transport with impurity charge scattering and phonon scattering was used to analyze the results. Non-monotonic charge transport was also observed in the temperature dependence of the residual conductivity (σ_r). Theoretical analysis of both σ and σ_r revealed a temperature independent contribution of $\sim 1.16\frac{e^2}{h}$ that is probably inherent to pristine graphene.

I. INTRODUCTION

Graphene is a two-dimensional zero bandgap semi-metal consisting of planar sp^2-bonded carbon atoms arranged in a hexagonal lattice.[1] It possesses a linear energy dispersion relation and exhibits an ambipolar electric field effect.[2–4] Pristine graphene is unstable in air as charged impurities are easily adsorbed during its growth and post processing.[3,5–8] In substrate supported graphene, these impurity charges are randomly attached to its top surface and at the graphene/substrate interface. Temperature-dependent charge transport measurements of graphene on Si^+/SiO_2 substrates with back gating show that the conductivity (σ) exhibits a positive and a negative temperature gradient depending on the graphene quality and carrier charge concentration.[9–14] In low mobility graphene (<3000 cm^2/V s) at or near the Dirac point (DP), σ had a positive temperature gradient over a wide temperature range, while far away from the DP there was a switch to a negative temperature gradient with increasing temperature due to an increase in the carrier concentration.[9]

We report on hole transport in low mobility graphene near the DP in the temperature range of 300 < T < 350 K. The graphene was deposited on Si^+/SiO_2 substrates, and a ferroelectric (FE) polymer thin film was used as the gate material in a field effect transistor (FET) configuration. Varying the gate voltage (V_G) polarizes the polymer, which compensates or uncompensates impurity charges at the polymer/graphene interface.[15] Impurity charges at the graphene/SiO_2 interface could also be affected, albeit weakly, by V_G. As the polarization varies when the temperature changes, both the impurity charge concentration (n_i) and the carrier charge density (n) vary, so they both are temperature-dependent. We suggest that these dependencies may explain the temperature dependence of the graphene conductivity observed in our experiments.

We note that we measured transport characteristics of graphene sample near the DP, but we avoided its immediate vicinity where

the electron–hole "puddling" distorts the σ vs V_G cone near its vertex, and the dependence of the charge carrier density n on the gate voltage V_G ceases to be linear. However, we worked with a "dirty" sample having low mobility and where the charged impurity concentration was high and, consequently, the cone distortion was pronounced only in close vicinity of the DP. Therefore, we could measure the conductivity σ at V_G sufficiently close to the Dirac voltage V_G^D still remaining in the region where n is the linear function of V_G.

Unlike previous studies, our results show that the temperature dependence of σ at the DP switched from having a positive temperature gradient to having a negative temperature gradient with increasing temperature. Thus, σ exhibits a switch from an "insulator-like" to a "metallic-like" behavior. The switch to a negative temperature gradient became weaker as one moved away from the DP. Using a FE polymer as the gate material, apart from trapping and compensating the impurity charges, can also tune the temperature at which the switch from a positive to a negative temperature gradient occurs by varying the gate voltage scan rate. In addition, a similar temperature dependence was observed for the residual conductivity (σ_r). This conductivity was defined at the intersection of the fits to the linear portions of the electron and hole branches in the $\sigma(V_G)$ curves as reported previously.[16]

In our experiments, the most important parameters (i.e., charge mobility) concerning the temperature dependencies of the conductivities σ and σ_r were obtained when V_G was not close to the coercive voltage (V_C) of the polymer gate, and specific effects occurring near $V_G \approx V_C$, such as rapid changes in the direction of the polarization, did not significantly affect the polymer gate specific capacitance C_i. Therefore, we omitted these effects from consideration and treated C_i as a constant.

We analyzed our data using a self-consistent theory for graphene transport[17] that was modified to consider the temperature-dependent n, which appears due to the temperature dependence of n_i. As is known, there exist several transport mechanisms in graphene, including activation across potential fluctuations created by charged impurities (which are responsible for inhomogeneous electron–hole puddle formation) and scattering by screened impurity charge and by phonons.[9,16–21] The activation mechanism is important at low impurity concentrations where the range of the potential fluctuations is higher, leading to a higher value of the activation energy.[17] For this mechanism to strongly contribute to the charge transport, the activation energy must exceed the thermal energy as, for example, in the experiments reported previously.[9]

In our experiments, the energy associated with carrier's activation across the potential fluctuations appears to be of the order of a few milli-electron volts, which is much smaller than the thermal energy within the considered temperature range. This gives us grounds to suggest that the graphene sample used in the experiments was a "dirty" one, characterized by a high n_i, where the effect of potential fluctuations was rather small. Therefore, we focus on diffusive transport that is mostly controlled by impurity charge scattering and phonon scattering.

II. EXPERIMENTAL

Graphene was grown via chemical vapor deposition and transferred onto a pre-patterned doped Si^+/SiO_2 substrate. No photolithography was involved once the transfer was complete; nevertheless, the fabrication process led to the adsorption of unintended impurity charges. Just these impurity charges dope graphene and act as dopants. Poly(vinylidene fluoride-trifluoroethylene) (PVDF-TrFE) (75/25), a room temperature ferroelectric co-polymer,[22] was used as the gate insulator and was spin-coated over graphene from a 9 wt. % solution in 1-methyl-2-pyrrolidinone. Fabrication details of the device are reported elsewhere.[15] Figure 1 shows a schematic diagram displaying the various components and the relevant electrical connections together with an optical microscope image of the actual device. The graphene channel length (L) and width (W) were 7 and 175 μm, respectively, while the PVDF-TrFE film thickness was 1.3 μm. A Keithley Model 6517A electrometer and a Keithley Model 2400 source meter were used for electrical characterization of the device in vacuum. The drain–source voltage (V_{DS}) was fixed at 100 mV, while the gate voltage (V_G) was scanned as follows: −40 → +40 → −40 V at a scan rate of 100 mV/s for each set point temperature. V_G was held at −40 V for 300 s to achieve uniform gate polarization and temperature stabilization prior to starting a new scan. The conductivity σ was calculated from the measured current using the expression $\sigma = \frac{L}{WR}$, where R is the graphene resistance. An Agilent Technologies Model 4294A Impedance analyzer was used to electrically characterize the polymer gate using a capacitor configuration.

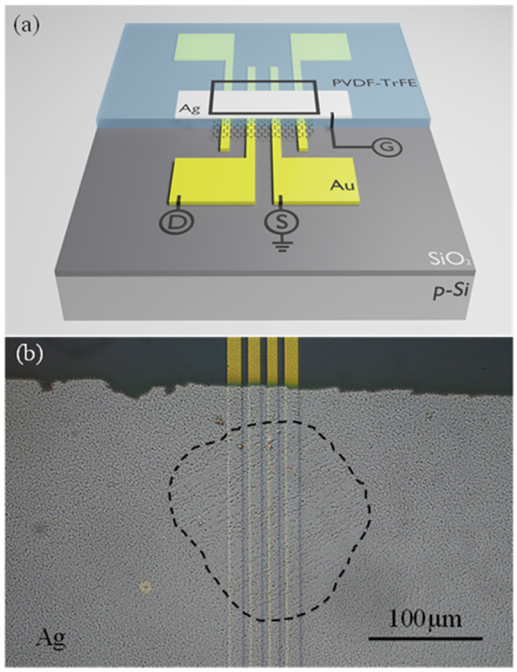

FIG. 1. (a) Schematic diagram of the graphene-based FE-FET showing the various device components and the associated electrical connections. S, D, and G are the source, drain, and gate terminals, respectively. (b) Top view optical microscope image taken within the black rectangle shown in (a) above for the actual device. The dashed black line indicates the outer edge of the graphene film that lies above the S/D electrodes and below the PVDF-TrFE film and the Ag gate electrode.

III. THEORETICAL ANALYSIS

Among many inherent features characterizing charge transport in graphene, two have been particularly discussed in the existing literature, namely, the transport in the immediate vicinity of the DP that is characterized by the low carrier density and the transport occurring farther away from the DP where the carrier density is higher. Within the first transport regime, a charge carrier density is mostly induced by the spatial inhomogeneity of the potential fluctuations caused by electron and hole puddles.[17,19] This induced carrier density n^* manifests itself as the widths of the plateaus in σ vs V_G plots corresponding to the minimum conductivity, and it is related to the activation energy (E_a) over these potential fluctuations. In the limit $n^* \to 0$, spatial inhomogeneities in the potential are smoothed and $E_a \to 0$.

It was suggested that the minimum conductivity occurs at the offset voltage $V_G^D = \frac{e\overline{n}}{c}$, where $\overline{n}$ is the added carrier density that compensates the average impurity potential and c is the specific capacitance of the substrate.[17,18] Both n^* and n depend on the impurity density n_i and these dependencies are thoroughly discussed.[17] In high carriers' density regime, the effect of potential fluctuations strongly reduces and the conductivity becomes linear in the carrier density and gives a mobility $\mu = \frac{\sigma}{ne}$.

A self-consistent theory for graphene transport shows that one may consider a graphene sample to be in the high carrier density transport regime when the relationship $n - \overline{n} > n^*$ is satisfied.[17] This may happen in a sufficiently dirty sample like that used in the present experiment because an increase in the impurity concentration results in higher values of n and lower values of n^*. Small values of activation energy extracted from the experimental data shown in Fig. 4 (see the inset) indicate that in the present sample, n^* is rather low, which gives grounds to expect that n is large enough to maintain the high carrier density transport regime. Note that even within this regime, the following expressions may not be employed to describe the conductivity at the very DP. However, we may use these expressions to explain our experimental data obtained near the DP.

Within this transport regime, the charge transport in graphene is a diffusive one, and the diffusive conductivity (σ_D) is determined by the following expression:[9]

$$\sigma_D(T) = \frac{e^2}{2}\int dED(E)v_F^2\tau(E,T)\left(-\frac{\partial f(E)}{\partial(E)}\right), \tag{1}$$

where $D(E) = \frac{2E}{\pi\hbar^2 v_F^2}$ is the density of states (DOS) of graphene, v_F is the Fermi velocity, and f(E) is the Fermi distribution function. The scattering time τ includes contributions from all relevant scattering mechanisms. In addition to the term given by Eq. (1), the expression for the graphene conductivity includes the temperature independent correction $\Delta\sigma$, which cannot be explained within the model of diffusive transport employed to get Eq. (1). This correction was introduced in some earlier works.[16,23] One may conjecture that $\Delta\sigma$ is related to inherent properties of pristine graphene.

In general, potential fluctuations created by the puddles reduce the DOS to a certain extent.[19] We assume that the reduced DOS $\widetilde{D}(E)$ may be described by

$$\widetilde{D}(E) = D(E)\exp\left(-\frac{E_a}{k_BT}\right). \tag{2}$$

Here, the activation energy E_a is related to the averaged range of the potential fluctuations, and it becomes zero in a homogeneous system. Low values of E_a observed in the present experiment enable us to neglect the difference between D(E) and $\tilde{D}(E)$ in further analysis.

As is known, in graphene samples at low temperatures, charge carriers are mostly scattered by charged impurities. This scattering mechanism strongly contributes at room temperature as well.[9,17,18,20] In addition, charge carriers in graphene are being scattered by phonons. It is noted[21] that the contribution from longitudinal acoustic phonons often is the most important since optical modes either are too weakly coupled to the charge carriers or have too high frequencies to serve as an efficient scattering channel. In general, scattering on surface optical phonons may give a noticeable effect in clean graphene samples on a SiO_2 substrate at room temperature.[9,24] However, in the present experiment, the impurity density is too high for this scattering mechanism to make a considerable contribution to transport. In further analysis, we take into account only two scattering mechanisms, namely, the scattering on the charged impurities characterized by the scattering time τ_i and the scattering on the acoustic phonons with the characteristic time τ_{ph}, and we have $\tau^{-1} = \tau_i^{-1} + \tau_{ph}^{-1}$. To choose appropriate approximations for these scattering times, we estimate the Fermi energy (E_F) for the graphene sample. As is known, $E_F = \hbar k_F v_F$ and the Fermi wave vector is related to the carrier charge density n: $k_F^2 = n\pi$. From here, one could derive the following expression for the Fermi temperature $T_F = \frac{E_F}{k_B}$: $T_F(K) \sim 1500\sqrt{n \times 10^{-12}}$, where n is expressed in cm^{-2}.[20] Assuming that we do not too closely approach the DP, we may find carrier densities n(T) from the relation

$$n(T) = \frac{\sigma(T)}{e\mu(T)} \tag{3}$$

using the experimental data for σ and μ. Within the considered temperature range, n(T) at the DP varies between $\sim 2 \times 10^{12}$ and 8×10^{12} cm^{-2}, as shown in Fig. 7(b), which corresponds to $T_F \approx 4000$–6000 K. Thus, the relationship $T \ll T_F$ remains valid over the whole temperature range considered in this work. As a first step, we omit the contribution from the scattering on phonons. Then, the following approximations for the diffusive conductivity given by Eq. (1) the scattering time τ_i could be obtained:[17,20]

$$\sigma_D = A\frac{e^2}{h}\frac{n}{n_i};\quad \frac{1}{\tau_i(E_F)} = \frac{2}{h}\frac{E_F}{A}\frac{n_i}{n}, \tag{4}$$

where for the graphene on a SiO_2 substrate, $A \approx 20$. Using this result, one may derive a simple expression for the impurity concentration n_i,[16,17]

$$n_i(T) \approx \frac{5\times 10^{15}(\mathrm{V\cdot s})^{-1}}{\mu(T)}. \tag{5}$$

The impurity concentration obtained using this formula is very high (of the order of 10^{12}–10^{13} cm^{-2}), which confirms that our sample is dirty, and the transport occurs within the large carrier density regime.

The low temperature approximation for τ_{ph} takes the form[21]

$$\frac{1}{\tau_{ph}(E_F)} = \frac{\pi}{4\hbar}\frac{n\Lambda^2}{\rho_m v_{ph}^2}\frac{T}{T_F}. \quad (6)$$

Here, Λ is the deformation potential characterizing electron–phonon interactions, ρ_m is the graphene mass density, and $v_{\rm ph}$ is the speed of sound in graphene. Comparing these results, we see that the phonon contribution to the total scattering time becomes more significant when both temperature and the carrier density increase.

The ratio $\frac{\tau_i}{\tau_{ph}}$ at $T \ll T_F$ may be presented as follows:

$$\frac{\tau_i}{\tau_{ph}} = \alpha A \frac{n}{n_i}\frac{T}{T_0}, \quad (7)$$

where the dimensionless constant $\alpha \approx 0.274$ and $T_0 = 1500$ K. The estimate for α is derived in the supplementary material.

Including into consideration the scattering on acoustic phonons, we present the expression for the diffusive conductivity in the form

$$\sigma_D = A\frac{e^2}{h}\frac{n}{n_i}\frac{1}{1+\frac{\tau_i}{\tau_{ph}}} = A\frac{e^2}{h}\frac{n}{n_i}\frac{1}{1+\alpha A\frac{n}{n_i}\frac{T}{T_0}}. \quad (8)$$

The practical expression for the graphene conductivity used to make fitting for the experimental curves is obtained by summing up the diffusive part given by Eq. (8) and the correction $\Delta\sigma$ inherent to the pristine graphene. The activation through the potential fluctuations is neglected in view of the smallness of its effect on the charge transport in the considered dirty sample. Thus, we have

$$\sigma = A\frac{e^2}{h}\frac{n}{n_i}\frac{1}{1+\alpha A\frac{n}{n_i}\frac{T}{T_0}} + \Delta\sigma, \quad (9)$$

where A and $\Delta\sigma$ are treated as fitting parameters. The residual conductivity σ_r is simply an extrapolation of the conductivity σ linear in the carrier density. Probably, there could be a qualitative difference in σ and σ_r temperature dependencies in clean samples where these fluctuations significantly affect charge transport. However, in the considered "dirty" sample, these effects are insignificant and σ_r is rather close to σ and reveals a similar temperature dependence shown in Fig. 7(a). Therefore, we use a similar expression to describe this quantity, namely,

$$\sigma_r = A\frac{e^2}{h}\frac{n_r}{n_i}\frac{1}{1+\alpha A\frac{n_r}{n_i}\frac{T}{T_0}} + \Delta\sigma. \quad (10)$$

The only difference between Eqs. (9) and (10) is the difference in carrier charge densities. The carrier density n_r is smaller than n, albeit moderately, as follows from the experimental data.

IV. RESULTS AND DISCUSSION

The complex dielectric permittivity ($\varepsilon^* = \varepsilon' - i\varepsilon''$) and polarization of the gate polymer were measured to support the data analysis discussed later. Figures 2(a)–2(d) show the frequency and temperature dependence of the polymer specific capacitance (C_i), polarization (P), and ε^*. From this figure, we note the following features: (i) The specific capacitance and polarization only slightly change in the temperature range of 300 < T < 350 K [see Figs. 2(a) and 2(b)]. (ii) This change is always in one direction (i.e., C_i slightly increases as temperature increases). (iii) The ferroelectric–paraelectric transition temperature (T_c) is 400 K [Fig. 2(c)]. (iv) There are no relaxations peaks in the temperature range of 300 < T < 350 K as seen in the dielectric loss plot of Fig. 2(d). These results are consistent for PVDF-TrFE with a 75/25 VDF/TrFE ratio.[25]

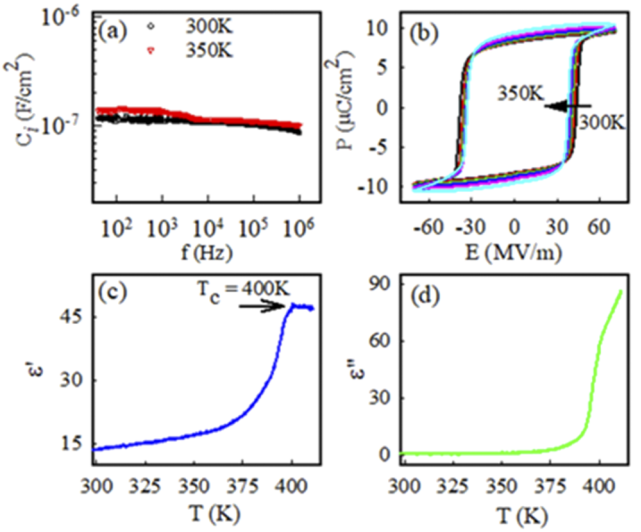

FIG. 2. (a) PVDF-TrFE specific capacitance vs frequency. (b) PVDF-TrFE polarization as a function of applied electric field. (c) Temperature dependence of the real part (ε') of the PVDF-TrFE dielectric permittivity. (d) Temperature dependence of the imaginary part (ε'') of the PVDF-TrFE dielectric permittivity. The complex dielectric permittivity was measured at a fixed frequency of 10 kHz.

In general, the specific capacitance of the FE gate dielectric may not be treated as a constant. However, since we are operating well below T_c and in a limited temperature range, the changes in the polymer specific capacitance do not exceed a few percent, as shown in Fig. 2(a). Therefore, in further analysis, we approximate C_i by a constant while analyzing the temperature dependence of σ. In addition, large changes in PVDF-TrFE (i.e., C_i, P, and ε^*) near T_c do not significantly affect our analysis and conclusions.

Figure 3 shows the σ vs V_G plot at three selected temperatures. Figure S1 in the supplementary material shows the σ vs V_G plots at all recorded temperatures during the heating run from 300 to 350 K. Referring, for example, to the red curve corresponding to 320 K, as V_G varies from −40 → +40 V, the conductivity passes through a minimum in the first quadrant, which corresponds to the Dirac point (DP-1) in graphene.[26,27] As V_G was scanned back to −40 V, σ remained relatively constant at the beginning since the gate polymer retains its polarization. As V_G was made more negative, the polarization decreased to zero and increased again in the opposite direction. The result was another DP-2 in the second quadrant. The electric displacement field (**D**) setup in the polymer by V_G was responsible for these effects. It contains a linear part (ε**E**) that dopes graphene with charge of the opposite sign and a hysteretic part (**P**) that can dope graphene with charge of either sign.[26] As V_G was varied, the competing effects of these two components gave rise to the anticlockwise/clockwise hysteresis and double minima indicated by red

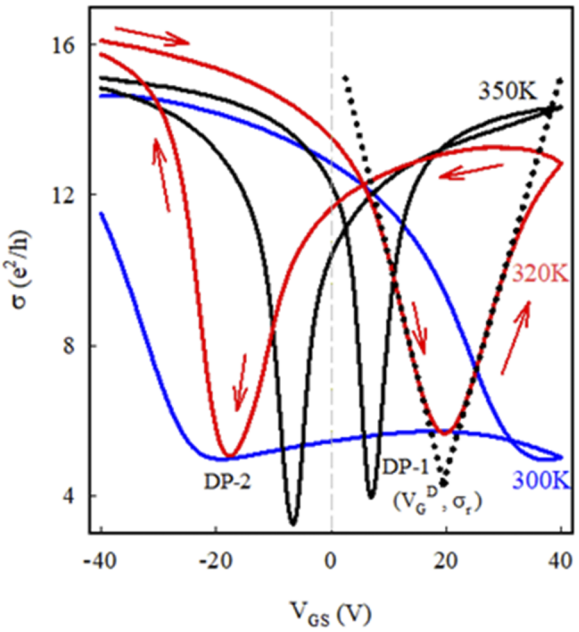

FIG. 3. Conductivity (σ) vs gate voltage (V_G) of the device at three selected temperatures: 300 (blue), 320 (red), and 350 K (black). The red arrows indicate the general direction of the current response as V_G is scanned from −40 → +40 → −40 V with a scan rate of 100 mV/s. The dotted lines are fits to the linear portions of the curve and are used to calculate the mobility (μ) while their intersection defines V_G^D and σ_r. DP-1 and DP-2 represent the two Dirac points in graphene when a ferroelectric material is used as the gate.

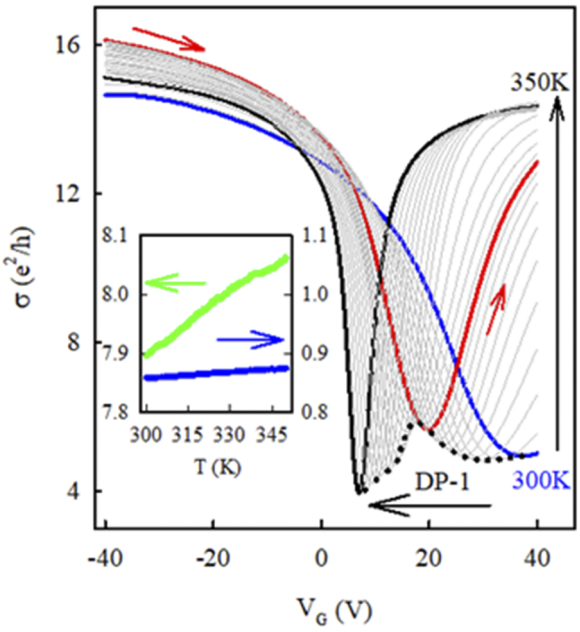

FIG. 4. Conductivity (σ) vs gate voltage (V_G) of the device at all recorded temperatures while heating from 300 to 350 K in steps of 2 K for forward bias (−40 → +40 V) gate voltages only. The colored plots are the same as those shown in Fig. 3. The thin gray lines are plots at the intermediate temperatures. The dotted curve traces the locus of Dirac points (DP-1) as temperature is increased. Inset: Conductivity (σ) vs Temperature (T) of two separate devices made of graphene that was transferred on to pre-patterned Si^+/SiO_2 substrates. (Blue) No PVDF-TrFE film over graphene. (Green) With a PVDF-TrFE thin film spin-coated over graphene. No gate voltage was applied to either device during the measurement.

arrows and are consistent with previous reports of FE gating on graphene.[15,26–31] During the V_G scan, in crossing any of the two DPs, the polarization flips its orientation, and the electrostatically doped majority carriers in graphene then change from holes to electrons or vice versa.

Figure 4, which was obtained from Fig. S1, shows the σ vs V_G curves at all measured temperatures during the forward gate scan (−40 → +40 V) only for purposes of clarity. We focus on hole transport, as that branch of the I_{DS}–V_G curves had well defined slopes over the entire temperature range. At and near the Dirac point, **P** approaches zero and doping by **E** was weak, given the low values of V_G and the relatively thick polymer film. Four features in this figure are evident as temperature was increased: (i) DP-1 shifts toward V_G = 0 V, i.e., *p*-doping weakens; (ii) the conductivity at the Dirac point (σ_{DP}) shows a peak where there is a change in the sign of the slope of σ(T); (iii) the mobility (holes and electrons) increases; (iv) the width (ΔV_{min}) of the conductivity minimum at the DP-1 gets narrower; and (v) σ_r remains close to that at the DP and shows a similar temperature dependence due to the narrowness of the plateaus at σ vs V_G curves. Figure S2 shows the σ vs V_G plots for the cooling run (350 → 300 K), albeit at a faster gate voltage scan rate (1 V/s) and confirmed the reversibility of the change in the temperature gradient of the conductivity from negative to positive and a tunable shift in the temperature at which this switch occurs. Tuning was possible because graphene doping by impurity charges via gate polarization was a non-destructive and reversible process.[15] The dotted-line fits to the linear portions of the σ vs V_G curve (in Fig. 3) yield the hole or electron mobility $\left(\mu = \frac{1}{C_i}\frac{d\sigma}{dV_G}\right)$, where C_i is the polymer specific capacitance (124 nF/cm^2), while the intersection of the two fitting lines defines the gate voltage (V_G^D) at the DP, and the residual conductivity (σ_r). Note that we can use this expression for μ as far as we remain in the region where σ is linear in V_G.

The inset of Fig. 4 shows the σ vs T plots of two different graphene devices on pre-patterned Si^+/SiO_2 substrates with and without a PVDF-TrFE coating. No gate voltage was applied to either device during characterization, and V_{DS} was 100 mV. The polarization in the PVDF-TrFE film, therefore, pointed in some random direction. These experiments were conducted to estimate the activation energy that influenced charge transport in graphene in the temperature range of 300 < T < 350 K. We assume an excess negative impurity charge concentration since all devices fabricated from graphene transferred onto Si^+/SiO_2 substrates that we tested had $V_G^D > 0$. The conductivity plots in the inset of Fig. 4, therefore, represent hole conduction away from the DP, and they both have a positive temperature gradient. Increasing the temperature leads to degassing, which eliminates some adsorbed impurities in the uncoated device, while in the PVDF-TrFE coated device, the impurity charges remain trapped. The temperature dependence of the conductivity in the uncoated graphene device should therefore be weaker when compared to the PVDF-TrFE coated device, as observed in the inset of Fig. 4.

Assuming an activation charge transport mechanism, we calculate an activation energy of 4.1 and 3.6 meV for the coated and uncoated device, respectively, which is much smaller than the thermal energy k_BT (k_B being the Boltzmann constant) within the considered temperature range. The observed weakness of the activation transport gives grounds to assume that the considered sample is characterized by a high carrier density n and high impurity concentration n_i. As we remain near but not too close to the DP, the impurity concentration is inversely proportional to the mobility. For graphene on the SiO_2 substrate, the relation between n_i and μ is given by Eq. (5).

Figure 5 shows the temperature dependence of n_i, which was calculated from Eq. (5), while Fig. 6 shows the temperature dependence of the hole mobility. Referring to Fig. 4, at 300 K (blue curve) and with $V_G = -40$ V, prior to the start of the scan, the FE gate was polarized up (↑), leading to a negative surface charge in the polymer at the polymer/graphene interface. This surface charge compensates positive impurity charges in its vicinity, resulting in an excess negative impurity charge concentration at the polymer/graphene interface that *p*-dopes graphene, and I_{DS} has a maximum value at this gate voltage. As V_G is scanned forward and approaches V_C, the change in polarization is gradual, lowering the doping effect and I_{DS} gets smaller, reaching its minimum value at DP-1 when $V_G = +37$ V. A positive gate voltage this large at the DP implies a high negative impurity charge concentration on graphene. The device on/off ratio was ~3. As $V_G \rightarrow +40$ V, the switched polarization does not reach saturation due to the quick start of the reverse gate scan and I_{DS} remains small as seen in Fig. 3 for the data corresponding to 300 K. Increasing the temperature assists FE domain alignment in the polymer, leading to sharper polarization switching;[23] V_G^D shifts toward $V_G = 0$ V and I_{DS} increases as $V_G \rightarrow +40$ V. The change in I_{DS} also gets steeper as V_G approaches V_C as seen in Fig. 4. At a given temperature, as V_G approaches V_C and the polarization gets weaker, it uncompensates some positive impurity charges that, in turn, compensate negative impurity charges in its vicinity. The net effect is to reduce the excess negative impurity charge that was present at the polymer/graphene interface at the start of the scan. Increasing the temperature facilitates charge compensation/uncompensation since the thermal energy brings charges closer together and homogenously redistributes the uncompensated charges. This reduces the excess negative impurity charge concentration even further. The result is a shift of the DP-1 toward $V_G = 0$ V, a narrowing of ΔV_{min}, and a decrease in n_i as temperature increases, as seen in Fig. 5. This is consistent with the observation that the DP is bound near V_C in FE-gated graphene transistors,[26–28] and V_C gets smaller with increasing temperature in PVDF-TrFE.[32]

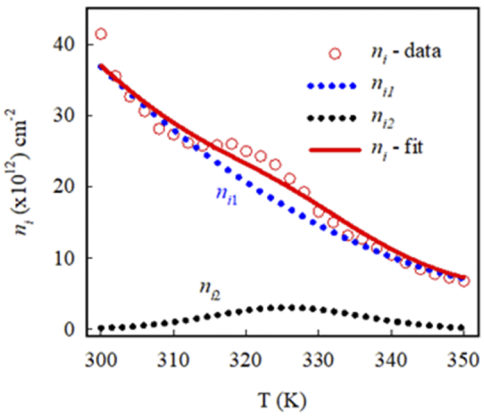

FIG. 5. Impurity charge concentration (n_i) vs Temperature (○) of the device. The data can be expressed as a sum of two contributions n_{i1} and n_{i2} (dotted lines). The solid line is the sum of these two contributions and fits the data. The fitting equations are given in the supplementary material.

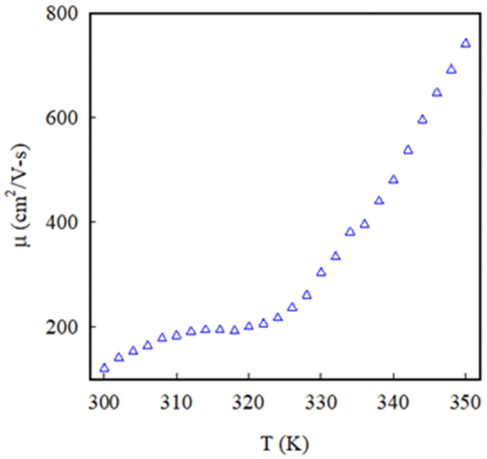

FIG. 6. Mobility (μ) vs temperature of the graphene FE-FET.

A closer look at n_i(T) in Fig. 5 shows a change in the curvature of the plot (red circles) at 324 K. To explain this feature, we present n_i as a sum of two separate charge concentrations: the impurity charge concentration at the polymer/graphene interface (n_{i1}) and the other at the graphene/SiO_2 interface (n_{i2}). The gate polarization that primarily compensates the impurity charges at the polymer/graphene interface controls n_{i1}. As seen in Fig. 4, V_G^D gets smaller as the temperature increases. This implies that the *p*-doping in graphene gets weaker. Thus, n_{i1} is a monotonously decreasing function of temperature as seen in Fig. 5 (blue dotted line). We propose that the temperature dependence of n_{i2} arises from the changing graphene–impurity charge separation. As temperature rises, since no back gate voltage is applied, these charges can approach the graphene surface effectively increasing n_{i2} and its doping effect on graphene gets stronger. However, above 324 K, the charges are close enough to the graphene surface that the induced charge carriers screen them, effectively decreasing n_{i2}. The result is assumed to have a Gaussian shaped temperature dependence as seen in Fig. 5 (black dotted line). The solid line is a fit to the data and is the sum of n_{i1} and n_{i2}. See the supplementary material for the equations used to determine n_{i1} and n_{i2}.

The charge mobility increases non-linearly as temperature increases, as seen in Fig. 6. A sharp increase near T = 324 K coincides with the temperature at which the minimum conductivity at the DP-1 reaches its peak value as shown in Fig. 4. The decrease in n_i following the temperature increase enhances the scattering time for the scattering on charged impurities (which is the most important transport mechanism in high carrier density graphene) and results in

an increase in the mobility. The non-linear profile of the μ vs T curve reflects the effect of the additional impurities with the density n_{i2}. As the temperature approaches T ~ 324 K from below, n_{i2} reaches its maximum values and we observe a plateau on the μ vs T curve, which is replaced by a quasi-linear portion at higher temperatures where n_{i2} becomes negligible.

A. Conductivity near the Dirac point

Figure 7(a) shows the temperature dependence of σ_r and for σ at three different values of ΔV, where $\Delta V = V_G - V_G^D$ measures the voltage difference from the DP. The conductivity was manually extracted from Fig. 4 for each ΔV and temperature T, where ΔV = 0 V corresponds to σ that was measured at the DP. As seen in Fig. 7(a), the conductivity has a positive temperature gradient at lower temperatures and switches to a negative temperature gradient near T ~ 324 K. As one moves away from the DP, the switch to a negative temperature gradient gradually weakens (Fig. S3). Figure 7(b) shows the temperature dependence of the carrier concentration ($n = \frac{\sigma}{e\mu}$) corresponding to each of the σ vs T plots shown in Fig. 7(a). We assume that the mobility shown in Fig. 6 is the same and use it to calculate n for the different conductivities. This assumption follows from the constant value of the specific capacitance that was used in the analysis.

Using the carrier concentration corresponding to σ at the DP (n_{DP}) as an example, the inset of Fig. 7(b) shows that similar to the impurity density n_i, the carrier concentration n_{DP} can be expressed as the sum of two separate contributions n_1 and n_2, respectively. The solid line is a fit to the data and is the sum of n_1 and n_2. In a similar manner, the carrier concentrations corresponding to other curves in Fig. 7(b) can also be expressed as sums of two terms like those mentioned above (see the supplementary material for the fitting equations). Knowing the temperature dependence of n_i (Fig. 5) and n [Fig. 7(b)], Eqs. (9) and (10) were used to fit the conductivity results shown in Fig. 7(a).

To understand the non-monotonicity of the conductivity at the DP in Fig. 7(a), the temperature dependence of the corresponding induced carrier concentration n_{DP} needs to be analyzed. The gate voltage and the impurity charge on the polymer/graphene interface electrostatically induce charges into graphene that contribute to n_1. The contribution n_2 results from doping by the thermally dependent graphene–impurity charge separation at the graphene/SiO_2 interface. Note that the net impurity charge concentration on the graphene surfaces was also presented as the sum of two terms $n_i = n_{i1} + n_{i2}$. As discussed before, these terms appear due to processes occurring at the graphene/polymer and graphene/substrate interfaces, respectively, and their temperature dependencies resemble those of n_1 and n_2.

At any instant and temperature, the following processes affecting diffusive charge transport are present at the polymer/graphene interface: (i) impurity charge (n_{i1}) compensation due to polarization of the gate polymer, (ii) impurity charge (n_{i1}) screening by charges associated with n_1, (iii) scattering of charges associated with n_1 by longitudinal acoustic phonons in graphene, and (iv) scattering of these charges by the impurities associated with n_{i1}. Except for the gate polymer polarization effect, the processes mentioned above are also present at the graphene/SiO_2 interface controlling the contributions n_{i2} and n_2. The interplay of these processes results in the temperature-dependent charge carrier concentration as well as the above discussed charged impurity concentration.

As shown in Fig. 5, n_{i1} falls when the temperature rises, whereas n_{i2} reaches a maximum near T ~ 324 K and smoothly drops when we move away from this temperature. In a similar way, the induced carrier density n_1 monotonically decreases with temperature as shown in the inset of Fig. 7(b). The Gaussian shape for the temperature dependence of n_2 (as well as that of n_{i2}) can be explained by considering the graphene–impurity charge separation at the graphene/SiO_2 interface. As temperature increases, the thermal energy acquired by the impurities reduces their distance from the graphene surface, which increases n_2 via doping. Above a certain temperature (324 K), however, the closer they get to graphene, the greater is the likelihood for them to be screened by charges carriers, thus reducing the concentration of the charge carriers that can actively participate in transport. The screening affects both contributions to the carrier

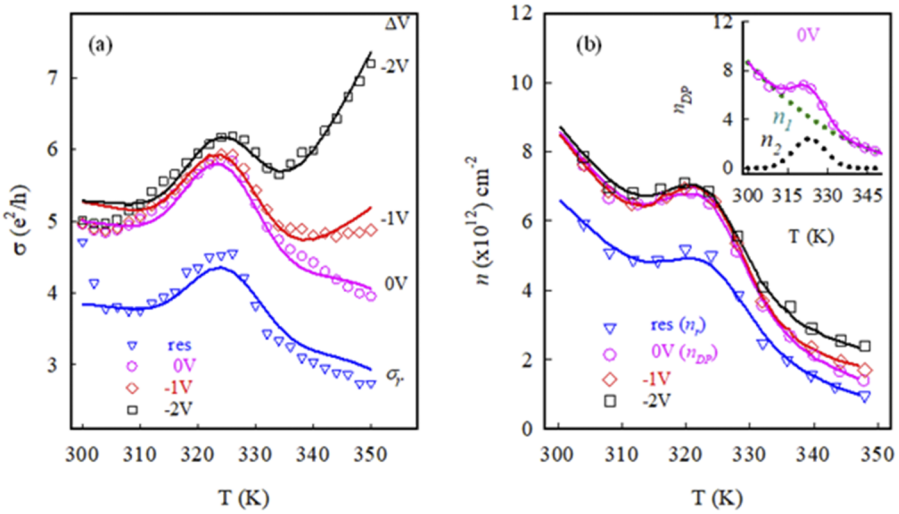

FIG. 7. (a) σ vs T for different values of ΔV. These data points were extracted from Fig. 4. ΔV = 0 V corresponds to σ measured at the Dirac point. σ_r is the residual conductivity. The solid lines are fits using Eqs. (9) and (10) in the text. (b) Carrier charge concentration (n) vs T for the same values of ΔV shown in (a). Inset: n_{DP} vs T for ΔV = 0 V, graphically showing that it can be expressed a sum of two concentrations: $n_{DP} = n_1 + n_2$. The solid lines are fits to the equations given in the supplementary material.

density, but it is especially pronounced in the temperature dependence of the smaller portion n_2, resulting in the Gaussian curve shown in Fig. 7(b).

The most important factor governing the behavior of the conductivity of "dirty" graphene at the DP given by Eq. (9) is the temperature-dependent ratio of n_{DP} and n_i. As follows from the present data, at lower temperatures, n_i falls faster than n_{DP} and we even observe a slight increase in $n_{DP} = n_1 + n_2$ with increasing temperature seen in the inset of Fig. 7(b). Therefore, the ratio $\frac{n_{DP}}{n_i}$ enhances as the temperature approaches 324 K from below, giving rise to the positive temperature gradient of σ. At higher temperatures, n_{DP} drops faster than n_i when the temperature rises and this ratio decreases causing the negative temperature gradient of conductivity. As the experiment was carried out on a "dirty" graphene sample where the effect of potential fluctuation is weak, σ_r appears to be rather close to σ and its temperature dependence follows that of the latter. The qualitative difference between the two giving a new insight into transport properties of a doped graphene may be expected in cleaner samples where potential fluctuations significantly affect the transport.

A deeper insight into the dynamic competition between processes governing charge transport in doped graphene is necessary to adequately explain the switch in the temperature dependence of $\frac{n_{DP}}{n_i}$, which is beyond the scope of the present work. Nevertheless, we remark that the charge carrier scattering on the charged impurities is more intensive at lower temperatures where both n and n_i take on greater values, and this transport mechanism is known to result in the positive temperature gradient of the $\frac{n_{DP}}{n_i}$ and the conductivity. At higher temperatures, when n and n_i are getting significantly lower, we may expect a relative weakening of this mechanism, which makes the effect of impurity charge screening and phonon scattering more pronounced. It may happen that these effects would predominate, leading to the appearance of negative temperature gradient of σ (and of $\frac{n_{DP}}{n_i}$) observed in the present experiment. The absence of a dielectric relaxation peak in PVDF-TrFE as seen in the temperature dependence of ε'' in the temperature range of 300 < T < 350 K [Fig. 2(d)] confirms that the peak seen in the charge density in Fig. 7(b) as a function of temperature is not influenced by any relaxation mechanism in PVDF-TrFE.

B. Conductivity away from the Dirac point

The temperature dependence of the carrier concentrations for $\Delta V = -1$ and -2 V as shown in Fig. 7(b) is similar to that at $\Delta V = 0$ V. Therefore, we may assume that the switch in the temperature gradient of σ is controlled by the same factors as those acting at the DP. As ΔV gets more negative, the impurity charge and induced carrier charge concentrations increase. Accordingly, charge carrier scattering on charged impurities strengthens. This results in gradual weakening of the negative temperature gradient in σ. The temperature gradient of conductivity becomes positive again at T > 340 K and remains so at higher temperatures, as seen in Fig. 7(a) and Fig. S3.

For $\Delta V = -1$ V, n_i(T) was assumed to be the same as that shown in Fig. 5 and applying Eq. (9) to analyze the data yielded a good fit as seen Fig. 7(a). It was, however, necessary to increase n_i(T) slightly for $\Delta V = -2$ V to get a good fit for the conductivity data shown in Fig. 7(a). This was justifiable since $\Delta V = -2$ V lies further away from the DP and **P** is not zero. Some positive impurity charges at the polymer/graphene interface therefore remain compensated. Thus, the excess negative impurity charge at $\Delta V = -2$ V will be slightly higher compared to that at the DP and will lead to a higher induced carrier concentration. The fitting parameters are shown in Table I, and the solid lines in this figure represent fits using Eqs. (9) and (10). Note that for all curves, the parameter A takes on values close to 20, which is the estimate obtained theoretically for graphene on the SiO_2 substrate,[9,16,17] assuming the scattering on screened charged impurities as the predominating transport mechanism. Presumably, it is valid in the considered case because the high impurity concentration in the sample weakens the effect of potential fluctuations, and the effect of phonons is rather small, although not negligible. In addition, the conductivity $\Delta\sigma$ ($1.16\frac{e^2}{h}$) has the same order as that reported in an earlier work.[17,33] This observation adds credibility to the tabulated A and $\Delta\sigma$ values.

TABLE I. Tabulated values of the fitting parameters as defined in the text.

σ as indicated in Fig. 7(a)	A	$\Delta\sigma$
Residual	18.2	1.06
$\Delta V = 0$ V	20.7	1.16
$\Delta V = -1$ V	22.8	1.16
$\Delta V = -2$ V	21.0	1.16

V. CONCLUSIONS

Charge transport near the DP in graphene with ferroelectric gating was investigated in the temperature range of 300 < T < 350 K. The experiment was carried out on a "dirty" graphene sample where the effect of electron–hole "puddling" was rather weak and the charge carrier density retained a linear dependence on the gate voltage everywhere except for the immediate vicinity of the DP. This provided us with an opportunity to measure conductivity still linear in V_G but close to that at the DP. The temperature dependence of the conductivity appeared to be similar to that at the DP. We observed a positive temperature gradient in the conductivity that switched to a negative temperature gradient at T ~ 324 K at the DP. The negative temperature gradient effect became weaker as one moved away from the DP. The most important factors that could control charge transport in a doped graphene, such as impurity charge scattering, phonon scattering, and impurity charge screening, were analyzed to explain the non-monotonic behavior of the conductivity. It was shown that the considered sample was characterized by a high concentration of charged impurities, resulting in the activation energy values of the order of a few milli-electron volts and indicating that the effect of potential fluctuations was weak. In the present experiment, charge transport was mostly diffusive, controlled by the scattering of charge carriers on screened charged impurities and, to a certain extent, by phonons.

The specific temperature dependence of the graphene conductivity reported in the present work appeared due to the effect of the FE polymer that trapped impurity charges at the polymer/graphene interface and compensated their charges via polarization of the polymer, thus changing the impurity charge concentration n_i and, thereby, the carrier density n. This compensation together with a

temperature-dependent graphene–impurity charge separation at the graphene/SiO_2 interface resulted at a temperature-dependent ratio of n and n_i that was responsible for the occurrence of a peak on the σ vs T curve at and near the DP.

A similar temperature behavior was observed for the residual conductivity σ_r. This is not surprising since, for "dirty" samples like that used in the experiment, the potential fluctuations become insignificant and the difference between σ and σ_r nearly vanishes. Nevertheless, we remark that studies of σ_r in cleaner samples and at lower temperatures could bring interesting results giving new insight into the transport properties of graphene.

Finally, using a FE polymer as the gate material allowed for tuning the temperature at which the gradient of the temperature dependence of σ switches from positive to negative, for example, by varying the gate voltage scan rate. The conductivity behavior was reversible, and the option of using a back gate voltage can enhance the device on/off ratio. This should give better control of impurity charge compensation/uncompensation by the polarized gate and further insight into charge transport near the DP.

SUPPLEMENTARY MATERIAL

See the supplementary material for a complete plot of the device curves at all temperatures and for additional equations as mentioned in the text.

ACKNOWLEDGMENTS

This work was supported by the National Science Foundation under Grant Nos. DMR-PREM-1523463, DMR-PREM-2122102 and DMR-RUI-1800262.

DATA AVAILABILITY

The data that support the findings of this study are available from the corresponding author upon reasonable request.

REFERENCES

[1] A. K. Geim and K. S. Novoselov, Nat. Mater. **6**, 183 (2007).
[2] K. S. Novoselov, A. K. Geim, S. V. Morozov, D. Jiang, Y. Zhang, S. V. Dubonos, I. V. Grigorieva, and A. A. Firsov, Science **306**, 666 (2004).
[3] K. S. Novoselov, A. K. Geim, S. V. Morozov, D. Jiang, M. I. Katsnelson, I. V. Grigorieva, S. V. Dubonos, and A. A. Firsov, Nature **438**, 197 (2005).
[4] A. H. Castro Neto, F. Guinea, N. M. R. Peres, K. S. Novoselov, and A. K. Geim, Rev. Mod. Phys. **81**, 109 (2009).
[5] L. Jiao, L. Zhang, X. Wang, G. Diankov, and H. Dai, Nature **458**, 877 (2009).
[6] G. Eda, G. Fanchini, and M. Chhowalla, Nat. Nanotechnol. **3**, 270 (2008).
[7] H. E. Romero, N. Shen, P. Joshi, H. R. Gutierrez, S. A. Tadigadapa, J. O. Sofo, and P. C. Eklund, ACS Nano **2**, 2037 (2008).
[8] Y. Yang, K. Brenner, and R. Murali, Carbon **50**, 1727 (2012).
[9] J. Heo, H. J. Chung, S.-H. Lee, H. Yang, D. H. Seo, J. K. Shin, U.-I. Chung, S. Seo, E. H. Hwang, and S. Das Sarma, Phys. Rev. B **84**, 035421 (2011).
[10] Y.-W. Tan, Y. Zhang, H. L. Stormer, and P. Kim, Eur. Phys. J.: Spec. Top. **148**, 15 (2007).
[11] J.-H. Chen, C. Jang, S. Xiao, M. Ishigami, and M. S. Fuhrer, Nat. Nanotechnol. **3**, 206 (2008).
[12] W. Zhu, V. Perebeinos, M. Freitag, and P. Avouris, Phys. Rev. B **80**, 235402 (2009).
[13] J. Yan and M. S. Fuhrer, Phys. Rev. Lett. **107**, 206601 (2011).
[14] J.-H. Chen, W. G. Cullen, C. Jang, M. S. Fuhrer, and E. D. Williams, Phys. Rev. Lett. **102**, 236805 (2009).
[15] K. S. Figueroa, N. J. Pinto, S. V. Mandyam, M.-Q. Zhao, C. Wen, P. Masih Das, Z. Gao, M. Drndić, and A. T. Charlie Johnson, J. Appl. Phys. **127**, 125503 (2020).
[16] J.-H. Chen, C. Jang, S. Adam, M. S. Fuhrer, E. D. Williams, and M. Ishigami, Nat. Phys. **4**, 377 (2008).
[17] S. Adam, E. H. Hwang, V. M. Galitski, and S. Das Sarma, Proc. Natl. Acad. Sci. U. S. A. **104**, 18392 (2007).
[18] E. H. Hwang, S. Adam, and S. D. Sarma, Phys. Rev. Lett. **98**, 186806 (2007).
[19] E. H. Hwang and S. Das Sarma, Phys. Rev. B **82**, 081409 (2010).
[20] E. H. Hwang and S. Das Sarma, Phys. Rev. B **79**, 165404 (2009).
[21] E. H. Hwang and S. Das Sarma, Phys. Rev. B **77**, 115449 (2008).
[22] T. Furukawa, Y. Tajitsu, X. Zhang, and G. E. Johnson, Ferroelectrics **135**, 401 (1992).
[23] M. Trushin and J. Schliemann, Phys. Rev. Lett. **99**, 216602 (2007).
[24] S. Fratini and F. Guinea, Phys. Rev. B **77**, 195415 (2008).
[25] H. Ohigashi, K. Omote, and T. Gomyo, Appl. Phys. Lett. **66**, 3281 (1995).
[26] Y. Zheng, G.-X. Ni, C.-T. Toh, M.-G. Zeng, S.-T. Chen, K. Yao, and B. Özyilmaz, Appl. Phys. Lett. **94**, 163505 (2009).
[27] X. Wang, Y. Chen *et al.*, Nanotechnology **29**, 134002 (2018).
[28] J. Heidler, S. Yang, X. Feng, K. Müllen, and K. Asadi, Solid-State Electron. **144**, 90 (2018).
[29] Y.-L. Sun, D. Xie, J.-L. Xu, X.-M. Li, C. Zhang, R.-X. Dai, X. Li, X.-J. Meng, and H.-W. Zhu, Carbon **96**, 695 (2016).
[30] H. J. Hwang, J. H. Yang, Y. G. Lee, C. Cho, C. G. Kang, S. C. Kang, W. Park, and B. H. Lee, Nanotechnology **24**, 175202 (2013).
[31] M. Hassanpour Amiri, J. Heidler, K. Müllen, and K. Asadi, ACS Appl. Electron. Mater. **2**, 2 (2020).
[32] W. J. Hu, D.-M. Juo, L. You, J. Wang, Y.-C. Chen, Y.-H. Chu, and T. Wu, Sci. Rep. **4**, 4772 (2014).
[33] P. M. Ostrovsky, I. V. Gornyi, and A. D. Mirlin, Eur. Phys. J.: Spec. Top. **148**, 63 (2007).